Journal of Alloys and Compounds 971 (2024) 172713

Contents lists available at ScienceDirect

Journal of Alloys and Compounds

journal homepage: www.elsevier.com/locate/jalcom

Surface two-dimensional hole gas in Si doped β-Ga_2O_3 thin film

Ekaterine Chikoidze [a,*], Jacob Leach [b,*], Zeyu Chi [a], Jurgen von Bardeleben [c], Belén Ballesteros [d], Anne-Marie Gonçalves [e], Tamar Tchelidze [f], Yves Dumont [a], Amador Pérez-Tomás [d,*]

[a] Groupe d'Etude de la Matière Condensée (GEMaC), Université Paris-Saclay, UVSQ – CNRS, 45 Av. des Etats-Unis, 78035 Cedex Versailles, France
[b] Kyma Technologies, Inc., 8829 Midway West Road, Raleigh, NC 27617-4606, USA
[c] Institut des Nano Sciences de Paris (INSP), CNRS UMR7588, Sorbonne Université, 4 place Jussieu, 75252 Paris, France
[d] Catalan Institute of Nanoscience and Nanotechnology (ICN2), CSIC and the Barcelona Institute of Science and Technology, Barcelona, Spain
[e] Institut Lavoisier de Versailles (ILV), Université Paris-Saclay, UVSQ – CNRS, 45 Av. des Etats-Unis, 78035 Cedex Versailles, France
[f] Faculty of Exact and Natural Science, Department of Physics, Ivane Javakhishvili Tbilisi State University, 3 Av. Tchavtchavadze, 0179 Tbilisi, Georgia

ARTICLE INFO

Keywords:
Gallium oxide
EPR measurements
Band bending
p-type conductivity
Surface analysis

ABSTRACT

Although two-dimensional electron gases have been realized in a number of semiconductor surfaces, examples of two-dimensional hole gases (2DHG) - the counterpart to 2DEG - are still very limited. Besides, owing to the deep energy level nature of potential dopants, achieving acceptor *p*-type β-Ga_2O_3 is a well-known challenge so far. In this work, we report what appears to be an exceptional *p*-type 2DHG surface on a Si-doped monoclinic (010) β-Ga_2O_3 crystal which otherwise is *n*-type in the bulk. The majority of the free carries at the surface have been determined to be holes with a sheet concentration of $p \sim 8.7 \times 10^{13}$ cm^{-2} and a puzzlingly high mobility value of $\mu_h \sim 80$ cm^2/(V·s) at room *T*.

1. Introduction

A highly conductive metallic gas that is quantum mechanically confined at a solid-state surface or interface is an efficient mechanism to improve the performances of advanced electronic devices enhancing channel conductivity or contact resistivity among others. Although two-dimensional electron gases have been realized in a number of conventional semiconductor surfaces AlGaN/GaN [1] (ZnO [2], In_2O_3 [3] examples of two-dimensional hole gases (2DHG), the counterpart to the two-dimensional electron gases, are still limited [4–8]. Examples of hole accumulation on the diamond surface [9] and these 2DHG ultra-wide bandgap (UWBG) devices include the *p*-channel two-dimensional hole gas associated with hydrogen-terminated (C-H) diamond FETs where the upward band bending indicates the presence of inversion layer without gate voltage [10]. Indeed, was proposed in 1947 that quantum confinement may be present at any semiconductor surface due to surface states [11]. A new generation of UWBG is being developed using Gallium Oxide rather than Diamond for power electronics and UV optoelectronics [12] and there also is a great interest in understanding and exploiting the unusual nature of Ga_2O_3 surfaces and interfaces [13]. This understanding will assist developers in the selection of optimal growth direction for epitaxial growth and/or improving final device's performance. There are some theoretical works dedicated to study different orientations of Gallium Oxide [14–16]. Experimentally, surface effects already reported have included the relationship between the hydroxyl termination and band bending at the (−201) surface of β-Ga_2O_3 bulk single crystals [17,18] and for the $(In_xGa_{1-x})_2O_3$ system [19]. While 2D channel p-type conductivity for Si doped Ga_2O_3 grown on sapphire substrate has been reported [20]. The thin films show a dominant *p*-type conductivity with room temperature mobility up to 7 cm^2/(V·s) and carrier concentration up to ~10^{20} cm^{-3}.

Here, we report unusual surface electronic properties of (010) oriented β-Ga_2O_3 homoepitaxial layers. For the (010) surface, there is only one termination, which contains all five atom types with two Ga_2O_3 units per surface unit cell per slab layer. Thus, the (010) orientation involves 10 atoms per layer unlike the (100). The local bonding on the (010) surface is found to resemble somewhat that of a layer of chemisorbed Ga_2O_3 "molecules" [16] The surface layer may be viewed as consisting of individual Ga_2O_3 units back-bonded to under-layer atoms, with no direct interaction between surface Ga_2O_3 units. The different oriented Ga_2O_3 surface energies were studied in detail and it was reported that (010) Ga(I)–O bonds in a GaO4 tetrahedron were stronger than those in a Ga(II)O6 octahedron, thus leading to higher surface energies [21] The combination of the special (010) surface orientation

* Corresponding authors.
E-mail addresses: ekaterine.chikoidze@uvsq.fr (E. Chikoidze), leach@kymatech.com (J. Leach), amador.perez@icn2.cat (A. Pérez-Tomás).

https://doi.org/10.1016/j.jallcom.2023.172713
Received 11 September 2023; Received in revised form 22 October 2023; Accepted 29 October 2023
Available online 2 November 2023

together with the combination of Si donor doping can lead the formation of a so called inversion space charge layer on the surface [22]. A range of physical characterization methods have been used to evidence that while the bulk and epitaxy are *n*-type in nature the top surface is degenerately *p*-type. The majority carriers on the 2DHG region are consistently determined as holes with a sheet concentration of $p \sim 6 \times 10^{13} - 10^{14}$ cm^{-2} in the temperature range of 80 – 700 K.

2. Results and discussion

2.1. Si doped β-Ga_2O_3 / (010) Ga_2O_3 thin films

β-Ga_2O_3 epilayers (shown in the inset of Fig. 1 (a)) were grown on 1" Fe-doped bulk (010) Ga_2O_3 substrates, which were prepared by Kyma Technologies. Prior to growth, the wafers were cleaned using solvents followed by hydrofluoric acid, and immediately loaded into a custom-designed vertical hydride vapor phase epitaxy (HVPE) reactor [23]. GaCl was generated in-situ by flowing Cl_2 over high purity metal gallium at 900 °C and dry air was used as the oxygen source for growth. The growth region of the HVPE reactor was held at 950 °C and 300 Torr, and SiH_4 was used as *n*-type dopant for the intentionally doped portion of the epilayer. Firstly, undoped Ga_2O_3 thin films of 600 nm were grown and then 200 nm Si doped films were deposited. Si content in the layers were measured by secondary ion mass spectroscopy (SIMS) measurement and estimated as [Si] = 1.2×10^{18} cm^{-3}. Fig. 1 (a) shows the grown structure. Theta-2Theta X-ray scans reveal only one reflection peak at 60° which corresponds to (020) growth direction. Transmission electron microscopy (TEM) image shown in Fig. 1 (b) indicates the existence of a different morphology of the topmost layer. The cross-sectional TEM analysis reveals a 20 – 40 nm layer on the top surface of the epi-layer which is structurally crystalline β-Ga_2O_3 but its density is significantly lower than in the bulk. Fig. 1 (c) shows transmission spectrum *T* [%] in the 200 – 2500 nm wavelength range. The Ga_2O_3 thin-films are transparent in UV–VIS–NIR.

2.2. Characterization of Si donor defects by EPR Analysis

Electron paramagnetic resonance (EPR) spectroscopy is a bulk technique, which measures the properties of the entire sample – substrate and epilayer, but its sensitivity is insufficient for the detection of surface related defects. Si, which introduces a shallow donor with a thermal ionization energy of $E_d = 36$ meV is paramagnetic when in the neutral charge state and can thus be investigated by EPR spectroscopy. Different EPR studies of Si donors in β-Ga_2O_3 have been reported [24–28] A particularity of the Si donor in β-Ga_2O_3 is that the EPR parameters are temperature and donor concentration dependent and allow a characterization of the conductivity processes. The temperature range in which the donor properties have been investigated is from $T = 4$ K to room temperature, covering the ranges from localization and thermal ionization into the conduction band.

As the crystal structure of β-Ga_2O_3 is monoclinic, the g-tensor is characterized by three principal values and principal axes, the orientation of which often do not coincide necessarily with lattice axes *a*, *b*, *c* of the crystal structure. The *g*-tensor identifies the spin $S = 1/2$ spectrum as the one of the neutral shallow Si donors. The linewidth of the SD spectrum varies strongly with temperature in distinct ranges corresponding to different conduction regimes (Fig. 2 (a) – (c)).

At low doping concentrations before impurity band formation, the SD is localized at low temperature ($T = 4$ K) and its linewidth is determined by inhomogeneous broadening due to dipolar interaction with the nuclear spins of ^{69}Ga, ^{71}Ga. It becomes delocalized at $T > 40$ K with hopping conductivity and in case of high doping beyond the Mott criterion. the formation of an impurity band. We have shown previously that the linewidth mimics the conduction regimes [27,28] and we have thus analyzed it in the same way. In Fig. 3 (a), we show the peak-to-peak linewidth as a function of temperature; it decreases from $\Delta B_{pp} = 7$ G at $T = 4$ K to below 0.2 G at room temperature. An analysis in the model of variable range hopping conduction (VRH) [29,30] implies a variation of the linewidth as $\Delta B = \Delta B_{00} \exp\left[-\left(\frac{T_0}{T}\right)^{0.25}\right]$.

Two temperature ranges between 17–50 K and 50–70 K with different slopes from which the parameter T_0 can be deduced. (Fig. 3 (b)) Their values are 6.6×10^4 and 4.4×10^6 respectively. Since for $T > 50$ K, thermal ionization into the conduction band will become important, only the lower temperature range will be analyzed for the VRH parameters.

The parameter T_0 is defined as $T_0 = \frac{\beta}{k_B D(E_F) a^3}$, from which we can deduce the concentration of localized states in the VRH temperature range $T = 20$ K to $T = 50$ K by $n(E_F) = 1/4 D(E_F) k_B T \left(\frac{T}{T_0}\right)^{-1/4}$ with $\beta = 18$ [29], $D(E_F)$ the density of localized states near the Fermi level, $a = 1.9$ nm the localization length assumed to be equal to the Bohr radius. We obtain a value of donor concentrations as 1.3×10^{18} cm^{-3}, which well corresponds to the Si doping level determined by SIMS.

2.3. Characterization of Si donors by capacitance-voltage measurement

Capacitance versus voltage (*C*–*V*) profile measurements were performed to determine ionized donor concertation in the epilayers. Fig. 4 (a) shows $1/C^2$ versus applied voltage bias with the slope corresponding *n*-type material. From this dependence, ionized donor concertation versus depletion length can be estimated as shown in Fig. 4 (b). Between 50 and 100 nm from the top of the epilayer surface, the ionized donor concertation can be estimated to be around 1.5×10^{18} cm^{-3}. Since Si

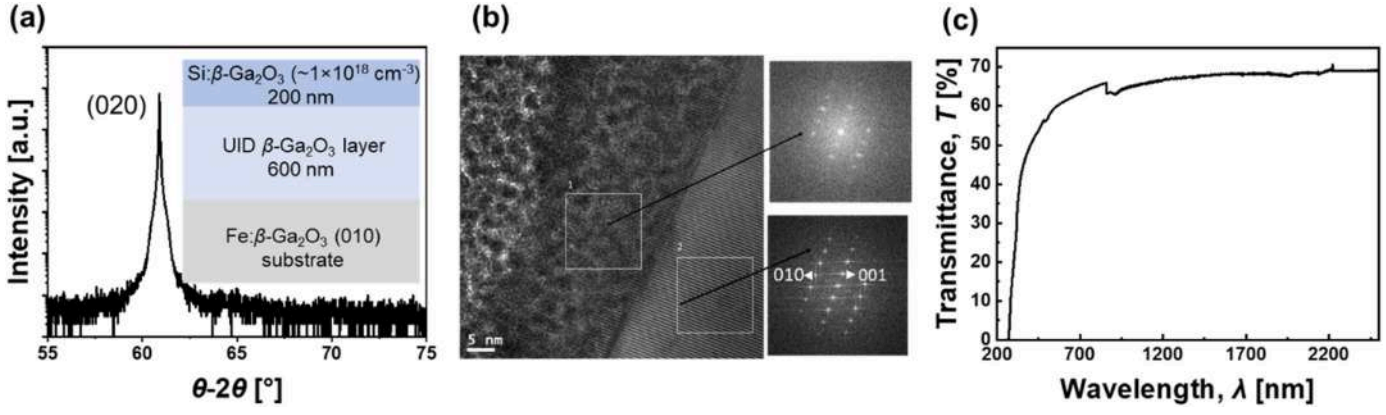

Fig. 1. (a) X ray diffraction Theta-2Theta scan. Insert: Sketch of grown epilayer structure. (b) Cross sectional TEM image of Si:Ga_2O_3 thin film with fast fourier transforms taken at the top of the epi-layer. (c) Optical transmittance at room temperature.

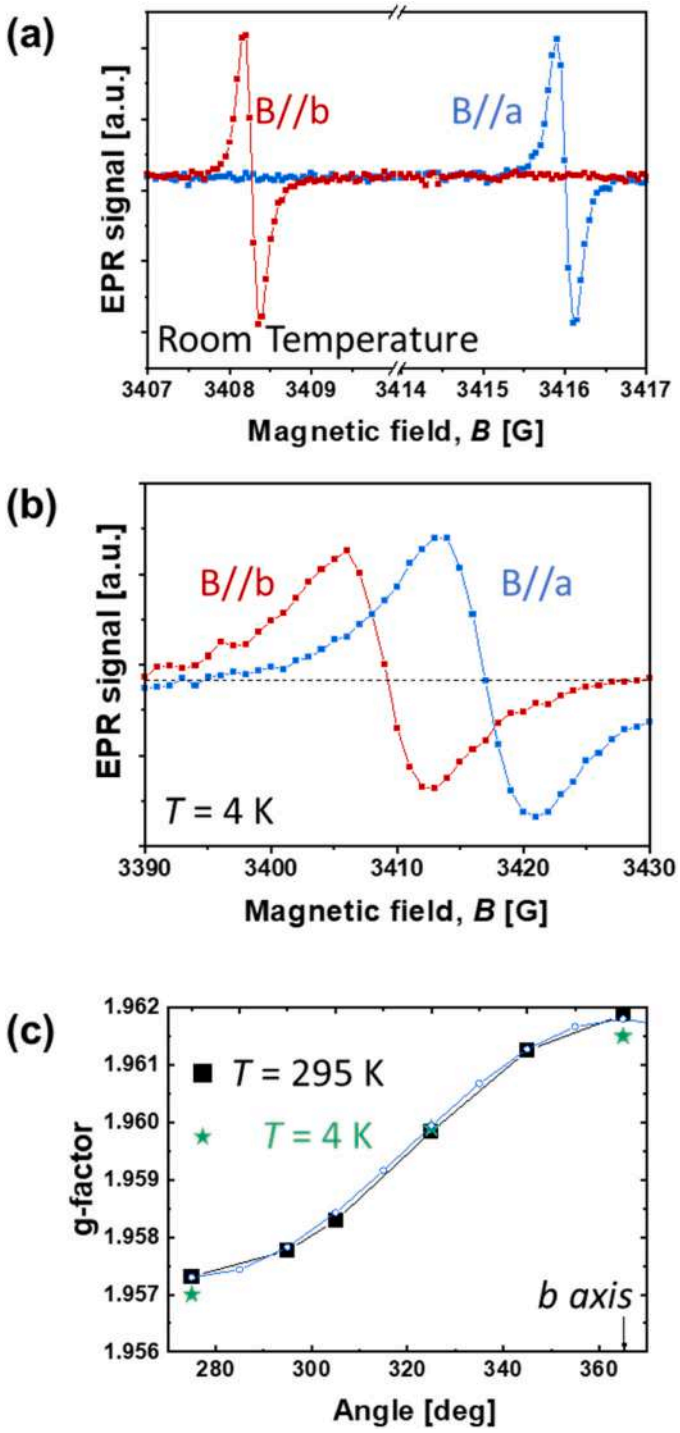

Fig. 2. (a) SD EPR spectra at room temperature for B//b and B//a, (b) at T = 4 K; (c) angular variation of the spin S = 1/2 spectrum g-values, which identifies it as a shallow donor.

ionization energy is known to be around 30 – 36 meV, at room temperature, free electron concentrations might be almost equal to the ionized donor concertation.

2.4. Surface chemical analysis: XPS, UPS and electrochemical measurements

2.4.1. Chemical nature of the acceptor surface: Formation of –OH (hydroxyl) groups

X-ray photoelectron spectroscopy (XPS) is a powerful and widely used technique for revealing the chemical nature of the Ga_2O_3 oxidation state and chemical atomic bindings at the very surface of our layers. The XPS spectra from the surface of a control sample (labeled *n*-type) of a 500 nm thick commercial (Novel Crystal Technology, Inc.) epiwafer of nominally *n*-type Si-doped β-Ga_2O_3 (N_d - N_a = 1.3 ×10^{18} cm^{-3}) grown on a single crystal β-Ga_2O_3 were used as a benchmark for our Si-doped epiwafer β-Ga_2O_3 crystal grown at Kyma (labeled *p*-type) core levels analysis. The samples were subjected to a standard solvent clean before analysis.

The room temperature normalized photoemission spectrum for the Ga2*p* and C1*s* core levels is shown in Fig. 5(a),(b). The XPS spectrum has been calibrated with respect to the adventitious species of C1s level energy at 284,8 eV following a standard procedure in particular when samples have allegedly different majority charge environment (either electrons and holes). The first overall observation is that the Gallium core levels are very similar, presenting no remarkable shifts in the core level binding energies (Fig. 5(a)). In general, the Ga2*p* signal is weaker (with respect to C1*s*) for the *p*-type which is ascribed to the more porous nature of the surface. The *n*-type sample presented a greater diversity of secondary peaks in the C1*s* spectra while the p-type virtually only displayed the one ascribed to C-C and O═C-O (Fig. 5(b)). The Ga2p doublet separation between the primary Ga2$p_{3/2}$ and the secondary Ga2$p_{1/2}$ was determined to be □Ga2*p*~26,7 eV for both samples. However, as shown in Fig. 5(c),(d), a Gaussian fitting of the (Ga2$p_{3/2}$) peaks reveal a slight broadening of the *p*-type sample when compared to the *n*-type reference. The subtraction of both profiles reveals an additional contribution on *p*-type centered at a binding energy 1117 eV which is ascribed to the formation of hydroxyl groups –OH [31]. To further corroborate the two main observations we have proceed to the analysis of the oxygen core level O1s. These two main observations were: (i) that the *n*-type and *p*-type core levels are structurally identical (as revealed by TEM) and (ii) that there is a formation of hydroxyl groups (-OH).

Fig. 6(a)-(d) shows the normalized O1s core levels of the surface of the *n*-type and *p*-type Ga_2O_3 crystals. The features of the oxygen peak has been split in four contributions: (i) The main Ga-O contribution from the Gallium-Oxide crystal binding (530,6 eV), (ii) O_{II}, a secondary peak owing to Gallium hydroxyl groups (Ga-OH) bonds (532,0 eV) [31], (iii) O_{III}, a secondary peak ascribed to other forms of –OH bonds (533,0 eV), probably adventitious [31]. (iv) O_{IV}, this last contribution (533,6 eV) is identical on both surfaces and is considered to be from adventitious C═O[32]. The deconvolution of the O1s peaks fixing their Gaussian peaks at exactly the same energy reproduces both, the *n*-type and *p*-type surfaces (Fig. 6(c)-(d)). This fact suggests therefore that both crystal surfaces are structurally identical but with different amount of hydroxyl groups. The subtraction of the *n*-type and *p*-type contributions is depicted in Fig. 6(b) where it can clearly be seen that the main difference comes from the Ga-OH bonds (a satellite at low binding energies is also reported in [31].

2.4.2. Analysis of the Fermi level by XPS and UPS and electrochemical measurements

X-ray photoelectron spectroscopy (XPS) and ultraviolet photoelectron spectroscopy (UPS) are suitable chemical methods to further investigate the main valence band characteristics of the top surface (~5 nm) of a crystal. While XPS uses soft X-rays to examine electrons in core-levels, UPS uses vacuum UV radiation to photo-excite the electrons in the valence band. When used in high resolution in the valence band vicinity (i.e., for the lowest binding energies), it is possible for XPS to directly detect whether there are states in the lower part of the bandgap (those responsible of the *p*-type character). As shown in Fig. 7 (a), a clear correlation was found within the amount of states in the lower half of the bandgap and the *p*-type character as compared with a reference *n*-type sample.

The reported contributions of the three different oxygen sites $O^{(1)}$, $O^{(2)}$, and $O^{(3)}$ is also shown in Fig. 7 (a). In the unit cell of β-Ga_2O_3 there are two different Ga sites as well as three different oxygen sites and the

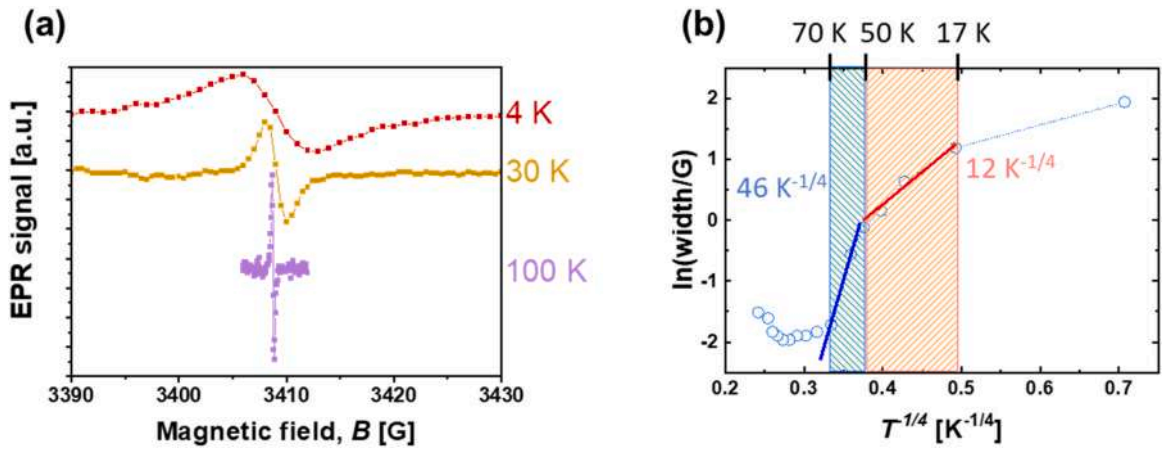

Fig. 3. (a) SD EPR spectra for three different temperatures; (b) variable range hopping (VRH) presentation ln(width) versus $T^{-0.25}$ from which the parameter T_0 can be deduced.

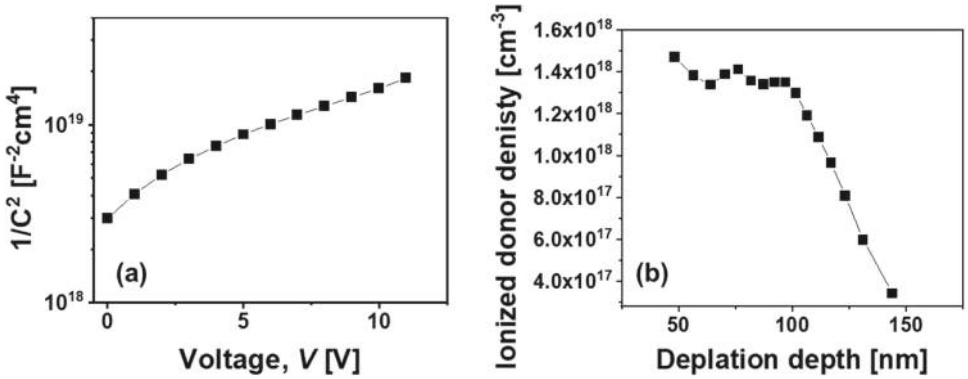

Fig. 4. (a) $1/C^2$ versus applied voltage bias (b) Ionize donor concertation versus depletion depth.

electronic structure is determined by the O2*p* states in the valence band (VB) and the Ga4*s*4*p* states which form the conduction band (CB) [33]. Accordingly, the strongest contributions in the first band below the VB maxima can be associated with the oxygen atoms at the tetrahedral Ga sites (BE ~ 6 eV, $O^{(1)}$). Michling and Schmeißer [34] suggested that the sequence of the three in-equivalent oxygen atoms in the VB spectra for the three bands are assigned in the sequence $O^{(3)}$, $O^{(2)}$, and $O^{(1)}$ where the strongest bonded oxygen atoms are those at the octahedral Ga sites (binding energy ~ 11 eV, $O^{(3)}$). In addition, the oxygen atoms with most pronounced covalent contributions are the $O^{(1)}$ states while $O^{(3)}$ states have a much smaller covalent contribution as they are reported to not contribute to the pDOS in the CB. When comparing the valence band profile of the Si-doped *p*-type vs. Si-doped *n*-type. it can be concluded that there is a relative weakening of the $O^{(2)}$ and $O^{(3)}$ (most covalent) oxygen coordination contribution when compared to $O^{(1)}$. The hybridation of these $O^{(3)}$ states with the gallium vacancies are suggested to be the source of the tail states and the predominant acceptor character of the surface. Among all combinations of paired vacancies, the creation of $V_{Ga}^{(1)}$-$V_O^{(1,2,3)}$ (tetrahedral) complexes is energetically more favorable than similar $V_{Ga}^{(2)}$-$V_O^{(1,2,3)}$ (octahedral) complexes.

Ultraviolet photoelectron spectroscopy (UPS) is in contrast commonly used to measure the kinetic energy of molecules irradiated with ultraviolet photons in the valence band from the very top surface (~0.5 – 1.5 nm) of the crystal. UPS allows direct measurement of the work function (*W*), determination of ionization potential position relative to Fermi/vacuum level, and yields a high-resolution VB cut-off in terms of counts (intensity). Compared to the previously analyzed *p*-type β-Ga_2O_3 samples [35] which were found to be mostly insulating at room temperature, the conductivity of the surface of the *p*-type hole gas is considered to be enough to avoid the undesired higher-binding energy shifts. As shown in Fig. 8, the UPS measurements straightforwardly corroborates the smaller Fermi level energy of our Si-doped sample compared to the *n*-type reference sample. From the experimental values of the Fermi level and the UPS secondary cut-off, it also possible to determine the different β-Ga_2O_3 crystal's work functions as $W = 3.15$ eV and $W = 5.71$ eV for the (reference) *n*-type and *p*-type Si-doped crystals, respectively. The ionization potential (i.e., the energy difference between the vacuum level and the VBM) was determined to be 7.65 eV and 6.21 eV for the (reference) *n*-type and *p*-type Si-doped samples, respectively.

Therefore, both XPS and UPS suggest that, in contrast to what was concluded from EPR measurements and *C–V* characterization for the bulk of sample, the top surface of Si:Ga_2O_3 epilayers is assumed to be *p*-type in nature. A smaller value of the Fermi level energy when comparing the reference *n*-type and *p*-type samples is pointed out by both techniques XPS and UPS. From UPS in particular, where the counts are larger than in XPS, the Fermi level (as derived from the first onset) seems to be as low as ~0.1 eV derived from UPS in log scale (Fig. 8(c)). This result suggests a degenerate state with high carrier concentrations at room temperature which is compatible with the hypothesis of the existence of a 2D hole gas at the surface of the thin film.

Such surprising results led us to study the surface conductivity by electrochemical measurements. Cyclic voltammograms were performed to study the surface conductivity and reactivity.

Interfacial electrochemistry studies are an appropriate method to understand fundamental processes occurring at a semiconductor (SC)/electrolyte junction. Like at the SC/metal junction, the SC/electrolyte junction also behaves as a Schottky barrier. The interfacial potential is

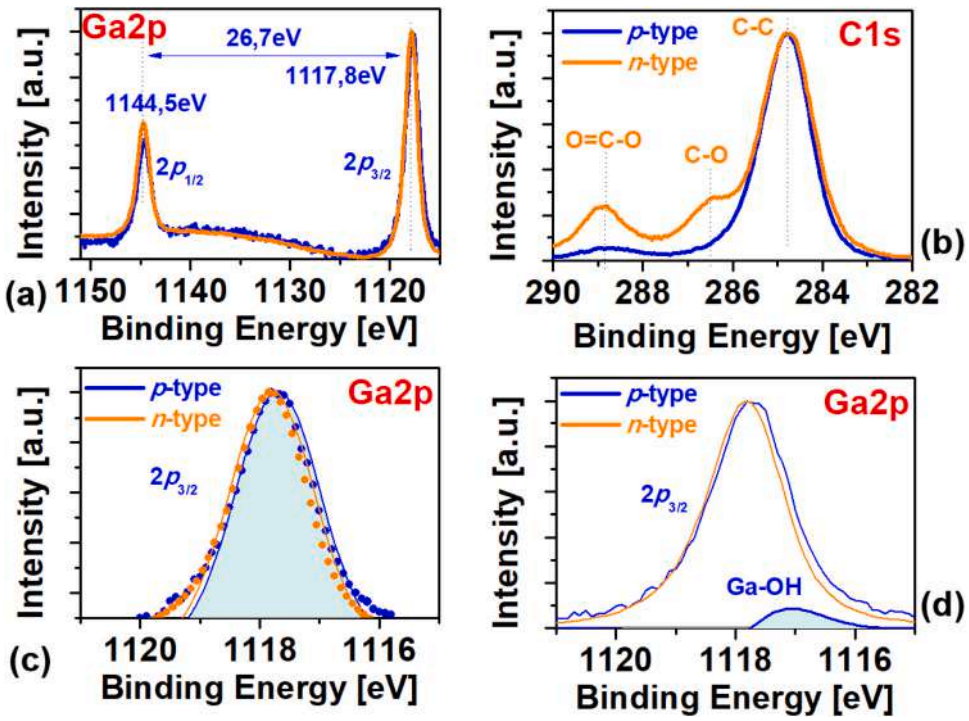

Fig. 5. X-ray photoelectron spectroscopy (XPS) of the Ga2*p* and C1*s* Ga_2O_3 core levels for a commercial Si-doped (*n*-type) reference and the Si-doped *p*-type surface of the crystal of this work. (a) Depiction of the Ga2*p* doublet. (b) C1s core level. (c) Ga2$p_{3/2}$ detail with Gaussian fitting. (d) Subtraction of the *n*-type and *p*-type contributions revealing hydroxyl Ga-OH groups.

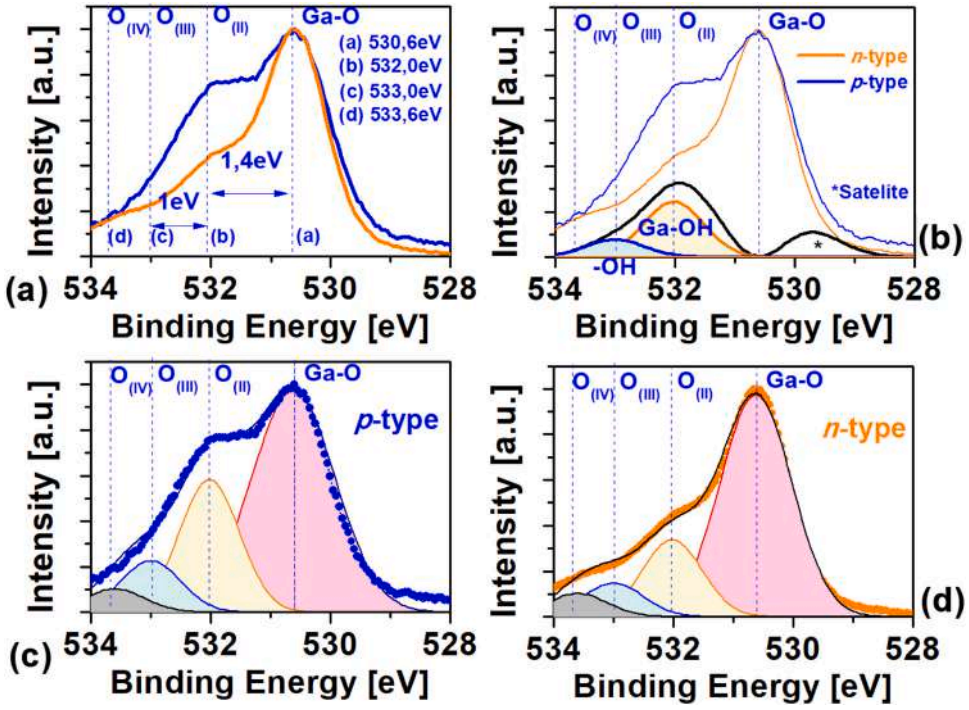

Fig. 6. X-ray photoelectron spectroscopy (XPS) of the O1*s* Ga_2O_3 core levels for a commercial Si-doped (*n*-type) reference and the Si-doped *p*-type surface of the crystal of this work. (a) Different suggested contributions of the O1s peak. Deconvolution of the (b) p-type and (c) *n*-type surfaces, respectively. (d) Subtraction of the *n*-type and *p*-type contributions revealing hydroxyl Ga-OH groups.

operated by a potentiostat using a classical three electrodes set-up. The polarization of the SC/electrolyte junction allows the control of the SC band bending in the space charge region of the SC. Several significant data of the junction are indeed obtained from electrochemical measurements. We can mention the determination of the open circuit potential and the range of applied potential which correspond to the depletion, accumulation and inversion layers of the SC. Impedance measurements give also access to the junction capacitance in which the SC capacitance can be identified [36]. It is necessary to underline that while physical capacitance-voltage measurement probes the epilayer in

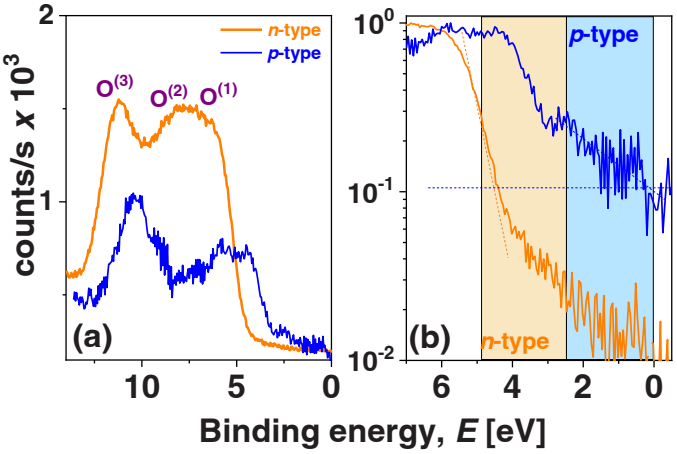

Fig. 7. (a) X-ray photoelectron spectroscopy (XPS) of the Ga_2O_3 valence band for a commercial Si-doped (n-type) reference and the Si-doped p-type surface of this work. The reported contributions of the three different oxygen sites $O^{(1)}$, $O^{(2)}$, and $O^{(3)}$ are also depicted. (b) A zoom of the normalized valence band edge region further evidencing the valence band tail states for the Si-doped p-type surface. The small value of the Fermi level indicates (~0.1 eV) that the surface is of semiconductor acceptor in nature and suggest accumulation of free holes at the top surface given the resolution of the technique (~5 nm).

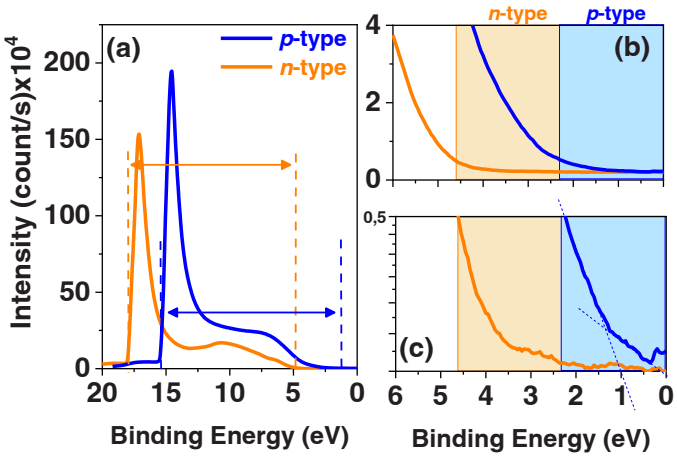

Fig. 8. (a) Ultraviolet photoelectron spectroscopy (UPS) of the Ga2O3 valence band for a commercial Si-doped (n-type) reference and the Si-doped p-type surface of this work. (b) and (c) A zoom of the valence band edge region depicting the shift towards smaller BEs Si-doped p-type surface. Again, the small value of the Fermi level indicates that the surface is of semiconductor acceptor in nature and suggest accumulation of free holes at the very top surface given the resolution of the technique (~1 nm).

the depth giving the donor distribution (Fig. 4 (b)), electro-chemical *C–V* method probe the free hole distribution near the surface.

All potentials are measured against a silver chloride electrode reference in saturated KCl aqueous electrolyte [37] A large smooth platinum electrode is also used as a counter electrode. The electrolyte is properly degenerated to avoid parasitic reaction with oxygen such as oxygen reduction mechanism at the interface Si:Ga_2O_3/aqueous electrolyte.

Interfacial impedance measurements are carried out in the dark at 1.03 kHz in a potential range where no significant faradic current is detected with a scan rate of 20 mV/s (Fig. 9 (a)). The graphical representation of Mott–Schottky describes the reciprocal of the square of capacitance (C^{-2}) versus the applied potential (Fig. 9 (b)). A very reproducible straight line is obtained over nearly two volts. At open circuit potential conditions, the equilibrium junction of Ga_2O_3/aqueous electrolyte made indeed the semiconductor in depletion region and the capacitance was directly related to the space charge layer of SC [38] The flat band potential is well defined and reproducible. The value is determined from the intercept of the regression line at the *x*-axis, and it is close to + 2 V vs. AgCl/Ag. From the slope sign (negative), we conclude that the junction SC/electrolyte behaves like a *p*-type meaning holes conductivity. This result shows again that the junction SC/electrolyte has a *p*-type behavior. We can firmly conclude that there is surface hole conduction in our epilayers.

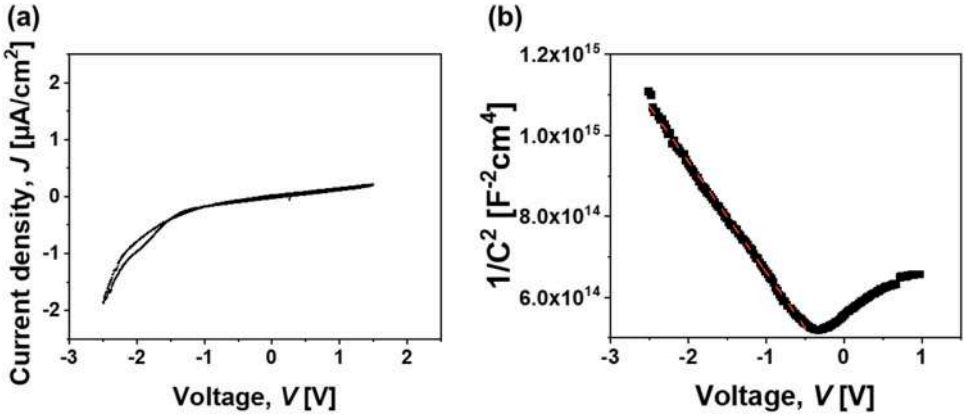

Fig. 9. (a) Cycle voltammetry. (b) Mott-Schottky straight line from impedance measurements.

2.5. Band banding

At the semiconductor surface, there may exist an electronic state which is different from bulk states. These states can be related to adsorbed molecules; or on a clean semiconductor surface, surface states may exist due to the termination of lattice periodicity at the surface [39]. These states may possess levels in the gap and consequently, be acceptor-like or donor-like, therefore they can change the statistical mechanics of the problem and modify the local equilibrium concentrations of electrons and holes in the near-surface region. When the concentrations of carriers change Fermi-level position relative to the band edges changes, and as the Fermi level position is independent of position, the energy bands must be displaced (bent). For band bending to occur, there needs to be charge transfer to equilibrate the Fermi level everywhere. This charge transfer then creates an electric field, and the associated potential shifts the bands in the vicinity of the charge transfer. The band bending direction is strongly dependent on both the surface and bulk defect levels. Transport properties of topological insulators: Band bending, bulk metal-to-insulator transition, and weak anti-localization Matthew [40].

In an *n*-type semiconductor, acceptor-like surface defects can receive electrons from the near-surface region; as a result, the surface becomes negatively charged. The picture is something like delta doping. The bands are bent upward [39] and the bending profile depends on how the electric field created by the surface charge is screened inside the semiconductor. This electric field can be screened by positively charged donors and/or by holes. The exact picture is defined by surface thermodynamics. If there are enough acceptor-like surface states, it must be energetically favorable that holes are the dominant species screening the surface negative charge (especially in near-surface regions). In this case inversion of conductivity type from *n* to *p* takes place in the pre-surface area, and the Fermi level goes below the valence band edge.

We modeled band bending for our epilayers using a Thomas-Fermi approach which very well describes the potential distribution in the cases when many electrons/holes are present in a limited area of space in order to define the position-dependent hole concentration and band bending profile. [41] Generally, the potential energy of holes is the near-surface area will the following sum:

$$V = V_f + V_h\# \tag{1}$$

Where V_f is the potential due to any fixed space-charge (charged defects) distribution, V_h is self-consistent part caused by mobile holes. The position dependent density of holes $p(z)$ is related to V through Poisson's equation:

$$\frac{d^2V}{dz^2} = \frac{e^2}{\varepsilon\varepsilon_0}\left[N_f(z) + p(z)\right]\# \tag{2}$$

Where $N_f(z)$ is the density of fixed charge; the z axis is perpendicular to surface, and directed towards the crystal interior. In the first approximation we neglect fixed charges, as fixed charges are usually distributed over length scales much larger than that for free carriers and give a weak contribution to the band bending. In this approximation:

$$\frac{d^2V}{dz^2} = \frac{d^2V_h}{dz^2} = \frac{e^2}{\varepsilon\varepsilon_0}p(z)\# \tag{3}$$

On the other hand, in degenerate limit, hole concentration is related to the distance between the Fermi level and valence band edge as

$$V(z) - E_F = \left(3\pi^2\right)^{2/3}\frac{\hbar^2}{2m_h^*}[p(z)]^{2/3}\# \tag{4}$$

As the fermi level position is unchanged, it is reasonable to choose the zero of energy to lie at E_F; Then combining (3) and (4), we get equation for band edge potential:

$$\frac{d^2V}{dz^2} = \frac{1}{3\pi^2}\left(\frac{e^2}{\varepsilon\varepsilon_0}\right)\frac{2m_h^*}{\hbar^2}V^{3/2}\# \tag{5}$$

The solution of this equation has the form:

$$V(z) = b\frac{1}{(z+z_0)^4}, b = \left(\frac{60\pi^2\varepsilon\varepsilon_0}{e^2}\right)^2\frac{\hbar^2}{2m_h^*}^3\# \tag{6}$$

Where z_0 is defined from the boundary condition $V = V_0$:

$$z_0 = (V_0/b)^{1/4}\# \tag{7}$$

If we substitute (6) in (4), we get the following expression for hole concentration:

$$p(z) = \frac{a}{(z+z_0)^6}, \text{with} a = \left(\frac{2m_h^*}{\hbar^2}\right)^{3/2}\# \tag{8}$$

In the calculation $m_h = 1.77\ m_0$ [42], static dielectric constant $\varepsilon_\square = 10$ [43] are used.

In Fig. 10, the dependence of hole concentration on z coordinate are given. The boundary condition to use: $V(0) = 4$ eV. We can see that on the top of the surface (within < 3 nm) hole densities are extremely high (> 10^{20} cm^{-3}) and then decreases to approximately to $p = 5 \times 10^{17}$ cm^{-3} when Z ~10 nm from the top of the surface.

2.6. Electrical transport properties

To find out more details about the electrical conductivity, Hall Effect measurements have been performed. Knowing that the majority of free carriers on the top of the Si:Ga_2O_3 layer is *p*-type we selected a Ti (50 nm)/Au (200 nm) contact structure, which was sputtered at each corner of the square shaped (1 ×1 cm^2) sample. *I–V* dependence at room temperature shows Ohmic characteristics (Fig. 11 (a)).

The electrical properties were measured from 80 to 750 K in a van der Pauw configuration with 6 months interval after keeping sample without any special protection. No significant change in sheet resistance were observed, which was around 7.2×10^2 Ω/sq at room temperature. Fig. 11(b) shows that sheet resistance does not varies very insignificantly throughout the 80 – 750 K temperature interval. Such metallic like (resistance decrease with temperature decrease) behavior indicates that sample might have very high concertation of free carries.

Hall Effect measurements were performed in the 80 – 750 K temperature interval repeated with 6 months intervals. As shown in Fig. 10 (a), the measured Hall voltage varied linearly with the perpendicularly applied magnetic field from − 1.6 to + 1.6 T at 300 K, indicating the *p*-type nature of the sample. When there is a two-layer structure, the inversion layer determines the electrical properties measured by the Hall effect. [44] The majority carriers are determined as holes with the sheet hole concentrations of $p = 8.7 \times 10^{13}$ cm^{-2} (Fig. 11 (a)). Thus,

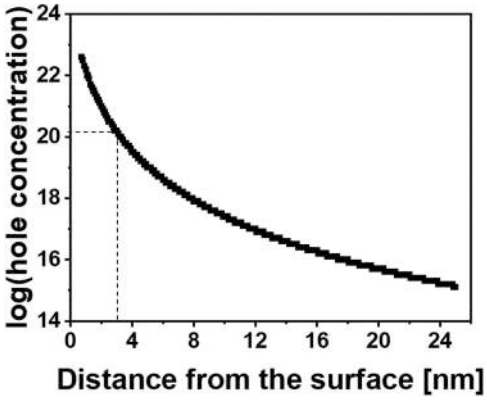

Fig. 10. Free hole concertation distribution versus Z, depletion region depth.

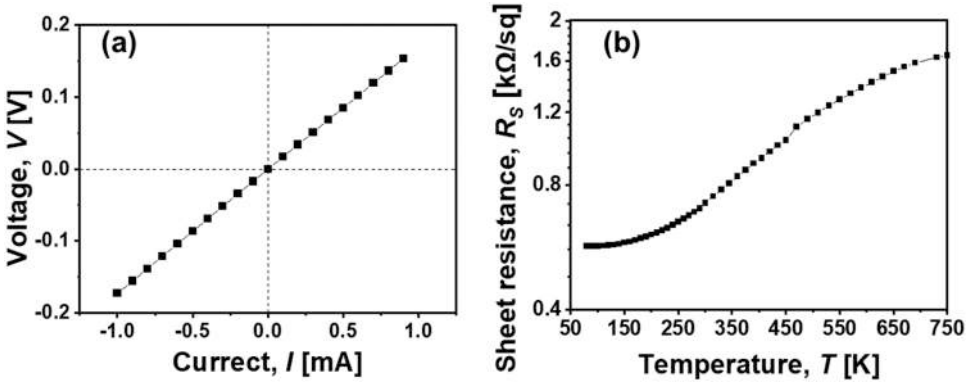

Fig. 11. (a) Current-voltage (I–V) dependence for electrical contact characterization at T = 300 K. (b) Sheet resistance versus temperature.

Hall Effect in coherence with XPS and ECV measurements confirms the surface *p*-type conductivity on the top of *n*-type in bulk Si:Ga_2O_3 epilayers. Such effect of changing of sign on the top surface opposite to the bulk conductivity type, ie. so called inversion layer creation due to the upward band banding on the surface, have been already observed for Mg:InGaN [45], InN [44], Rd doped SiO_2 [46], Ce doped SiO_2 [47], Iron pyrite [48] and recently for β-Ga_2O_3, when Au nanoparticles at the surface was responsible for the formation of an internal depleted region and *p*-type conductivity at the surface [49].

Carrier excess contributes to the conductance of the sample in a direction parallel of the surface. Thus, the mobilities measured by Hall Effect are so called "effective surface motilities μ_s" of the excess majority carriers. Measured mobility varies between $\mu = 164 - 40$ $cm^2/(V{\cdot}s)$ in the 80 – 750 K temperature range (Fig. 12 (b)). The actual value of effective mobility depends on the behavior of the carriers when they encounter the surface of the sample. A given carrier can retain its initial momentum in the direction parallel of the surface, or may suffer a change in this component of its spectrum. [22] Thus, the average behavior of all the carriers may range between completely specular reflection and "completely diffusive scattering", in which parallel momentum becomes randomized. It has been reported that the hole conduction mass in Ga_2O_3 is, indeed, fairly anisotropic and can be as low as ~0.4 m_0 for certain orientations (while larger than 10 m_0 in others). According to the authors, the low effective mass of the holes can be expected if conduction takes place along *b* or *c* crystallographic axis [42]. That corresponds to the (010) plane. Thus, high values of mobility for our sample can be explained by low effective mass in this crystallographic direction.

The *p*-type inversion layer on the top of *n*-type Si:Ga_2O_3 epilayers with the extraordinary high hole concentrations and surprisingly high mobilities can be considered as surface 2D hole gas (2DHG) as illustrated (Fig. 13). We know (by testing other sample) that this effect is not observable when Si doping level was less than 10^{18} cm^{-3}

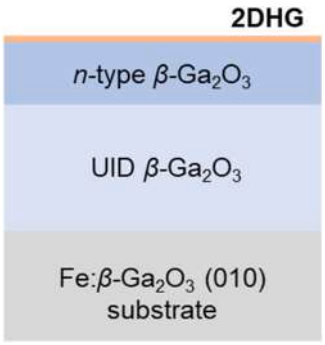

Fig. 13. Schematic illustration of epilayers and 2DHG.

3. Conclusion

A bi-layer of epitaxial Monoclinic β-Ga_2O_3 was grown on 1″ Fe-doped bulk (010) β-Ga_2O_3 substrates by hydride phase epitaxy consisting of 200 nm Si-doped (1.2×10^{18} cm^{-3} as determined by SIMS) onto 600 nm (UiD). XRD and Raman confirmed the monophasic and epitaxial nature. TEM inspection however revealed a ~20 – 50 nm surface termination region with apparent lower atomic density but yet perfectly β-Ga_2O_3 crystalline and epitaxial. *Bulk* EPR analysis revealed Si-donor signatures (in the neutral charge state Silicon is paramagnetic) with estimated donor concentrations of $\sim 1.3 \times 10^{18}$ cm^{-3}. In agreement with EPR and SIMS, capacitance-voltage (C-V) characterization also provided an ionized donor density of $\sim 1.5 \times 10^{18}$ cm^{-3} in the range of ~50 – 100 nm from the surface. However, surface techniques such as valence band analysis of XPS, UPS and electro-chemical *C–V* suggested that the epilayer surface was *p*-type in nature. Hall effect and Seebeck measurements corroborated the apparent *p*-type majority free carrier

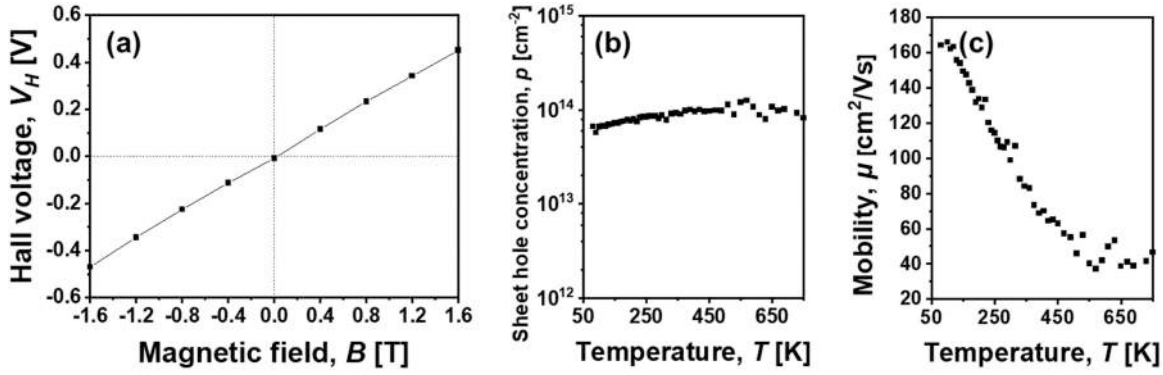

Fig. 12. (a) Hall voltage versus perpendicularly applied magnetic field at 300 K. (b) Hall hole density and (c) Hall mobilities versus temperature.

conductivity. The Hall sheet concentration and mobility were determined to be as high as 8.7×10^{13} cm^{-2} and 80 cm^2/Vs at room T (164 cm^2/(V·s) at 80 K). A Thomas-Fermi model suggests that on the top surface (< 3 nm), the free hole densities are extremely high (> 10^{20} cm^{-3}) decreasing to approximately $p = 5 \times 10^{17}$ cm^{-3} at 10 nm from the top surface and, therefore, resulting in what appears to be a two-dimensional hole gas (2DHG).

The surface-state-induced 2D electron gas (2DEG) on bare surface has been observed in InAs[50] and SrTiO3 [51,52] has been successfully studied by angle resolved photoelectron spectroscopy (ARPES). Yet, the resulting surface and interface 2DEGs all display similar electronic transport phenomena, suggesting a common underlying electronic structure defined by the properties of material and the crystallographic orientation of the surface or interface. Interestingly, Polyakov *et al.* [53] reported the anomalous electrical behaviors of the AlN/κ-Ga_2O_3 heterojunction, which the authors attributed to the presence of a 2DHG at the interface, formed due to the difference in spontaneous polarizations between AlN and κ-Ga_2O_3.

The further deep study of the surface of our (010) oriented Si:Ga_2O_3 will put a light on the origin of a band bending potential induced quantum confined 2DHG and challenges our current understanding of this ultra-wide bandgap semiconductor and open new prospects for advanced devices for power and UV optoelectronics.

4. Material and methods

4.1. Transmission electron microscopy (TEM) measurements

Crystallographic characterization and imaging were conducted using a field emission gun FEI Tecnai F20 microscope at 200 kV with a point-to-point resolution of 0.24 nm. Energy dispersive X-ray (EDX) and electron energy loss spectroscopy (EELS) spectrum images and profiles were obtained in high angle annular dark-field (HAADF) STEM mode with an EDAX super ultra-thin window (SUTW) X-ray detector a Gatan Quantum SE 963 imaging filter respectively. TEM cross-sections were prepared by conventional mechanical polishing and ion milling.

4.2. Secondary-ion mass spectrometry (SIMS) measurements

SIMS measurements were performed using a Cameca IMS 7 f equipment onto the samples to access the concentration and depth distribution of Zn dopant.

Raman spectra was recorded using Horiba Jobin Yvon Labram HR 8500, 514.5 nm excitation wavelength.

4.3. Optical transmittance/reflectance measurements

Optical transmission and reflectance spectra were measured in the 200 – 2500 nm wavelength range with a step of 2 nm using a Perklin Elmer LAMBDA 950 spectrophotometer.

4.4. Electron paramagnetic resonance (EPR) measurements

The EPR measurements were done with a commercial X-band spectrometer (Bruker) operating at 9 GHz and a variable temperature cryostat, which allowed to vary the temperature in the range $T = 4 – 300$ K. The magnetic field range was 0–1.7 T. The EPR spectra have been measured for a rotation around the crystal c-axis, which contains in particular the orientation of the applied magnetic field parallel to the b-axis and the a-axis.

C-V profile measurements were performed using a Hg-probe (Materials Development Corporation, Model 802B) in a top-top configuration with a 650-micron wide Schottky contact. Capacitance was measured using an HP 4275 A LCR meter with a 50 mV signal at 100 kHz in the parallel circuit mode configuration.

4.5. X-Ray Photoelectron Spectroscopy (XPS) and Ultraviolet Photoelectron Spectroscopy (UPS)

XPS and UPS were performed with a Phoibos 150 analyzer (SPECS GmbH, Berlin, Germany) in ultra-high vacuum conditions (base pressure 3×10^{-10} mbar). XPS measurements were performed with a monochromatic Al Ka X-ray source (1486.74 eV). UV source and monochromator for He I (21.2 eV) and He II (40.8 eV).

4.6. Electrochemical measurement

A classical three-electrode configuration, controlled by a Parstat 2273 potentiostat-galvanostat is used to perform cycle voltammetry (CV) in acidic aqueous solution ($[H_2SO_4] = 0.5$ M). Electrochemical experiments were performed in dark using the three electrodes set-up PARSTAT 2273 potentiostat/galvanostat. Pt wire and 1 mol dm^{-3} KCl silver/silver Chloride (Ag/AgCl, $E^\circ = 199$ mV vs. SHE) electrode respectively served as counter and reference electrodes. Zn doped Ga_2O_3 thin film was used as working electrode.

4.7. Hall effect measurements

Ohmic contacts were prepared by Ti/Au metal deposition by RF sputtering at the four corners of the sample. Hall Effect measurements were performed by home built high impedance high temperature setup in a van der Pauw configuration in the temperature range of 80 – 800 K applying the magnetic fields perpendicularly to the film plane varying from 0 to 1.6 T.

CRediT authorship contribution statement

Ekaterine Chikoidze: Conceptualization, Electrical transport measurements, Validation, Writing – review & editing. **Jacob Leach**: Thin films growth, X-ray analysis, C-V measurements, Writing, Conceptualization. **Zeyu Chi**: I-V, Hall Effect measurement, Data curation, Otical transmittance measurements, Writing. **Jurgen von Bardeleben**: EPR measurements, Investigation. **Belén Ballesteros**: TEM measurements. **Anne-Marie Gonçalves**: Electrochemical measurements and analysis. **Tamar Tchelidze**: Theoretical calculations, Conceptualization. **Yves Dumont**: Investigation, Optical measurements, Writing – review & editing. **Amador Pérez-Tomás**: Conceptualization, XPS-UPS analysis, Writing – review & editing.

Declaration of Competing Interest

The authors declare that they have no known competing financial interests or personal relationships that could have appeared to influence the work reported in this paper.

Data availability

Data will be made available on request.

Acknowledgements

The present work is a part of “GALLIA” International Research Project, CNRS, France. GEMaC and INSP colleagues acknowledge financial support of French National Agency of Research (ANR), project “GOPOWER”, CE-50 N0015–01. ICN2 is funded by the CERCA programme / Generalitat de Catalunya and by the Severo Ochoa Centres of Excellence programme, Grant CEX2021–001214-S.

References

[1] Halide vapor phase epitaxial growth of - Ga2O3 and -Ga2O3 films,J.H.Leach,APL Mater. 7, 022504 (2019); ⟨https://doi.org/10.1063/1.5055680⟩.

[2] L.F.J. Piper, A.R.H. Preston, A. Fedorov, S.W. Cho, A. DeMasi, K.E. Smith, Direct evidence of metallicity at ZnO (000 1 ¯) − (1 × 1) surfaces from angle-resolved photoemission spectroscopy, Phys. Rev. B. 81 (2010), 233305, https://doi.org/10.1103/PhysRevB.81.233305.

[3] V. Jovic, S. Moser, A. Papadogianni, R.J. Koch, A. Rossi, C. Jozwiak, A. Bostwick, E. Rotenberg, J.V. Kennedy, O. Bierwagen, K.E. Smith, The Itinerant 2D Electron Gas of the Indium Oxide (111) Surface: Implications for Carbon- and Energy-Conversion Applications, Small 16 (2020), 1903321, https://doi.org/10.1002/smll.201903321.

[4] H. Lee, N. Campbell, J. Lee, T.J. Asel, T.R. Paudel, H. Zhou, J.W. Lee, B. Noesges, J. Seo, B. Park, L.J. Brillson, S.H. Oh, E.Y. Tsymbal, M.S. Rzchowski, C.B. Eom, Direct observation of a two-dimensional hole gas at oxide interfaces, Nat. Mater. 17 (2018) 231–236, https://doi.org/10.1038/s41563-017-0002-4.

[5] M. Caironi, A solution for two-dimensional hole gases, Nat. Mater. 20 (2021) 1311–1312, https://doi.org/10.1038/s41563-021-01078-0.

[6] N. Kasuya, J. Tsurumi, T. Okamoto, S. Watanabe, J. Takeya, Two-dimensional hole gas in organic semiconductors, Nat. Mater. 20 (2021) 1401–1406, https://doi.org/10.1038/s41563-021-01074-4.

[7] Y. Chen, N. Pryds, 2D hole gas seen, Nat. Mater. 17 (2018) 215–216, https://doi.org/10.1038/s41563-018-0025-5.

[8] L.D. Anh, S. Kaneta, M. Tokunaga, M. Seki, H. Tabata, M. Tanaka, S. Ohya, High-mobility 2D hole gas at a SrTiO $_3$ interface, Adv. Mater. 32 (2020), 1906003, https://doi.org/10.1002/adma.201906003.

[9] K. Hirama, H. Takayanagi, S. Yamauchi, J.H. Yang, H. Kawarada, H. Umezawa, Spontaneous polarization model for surface orientation dependence of diamond hole accumulation layer and its transistor performance, Appl. Phys. Lett. 92 (2008), 112107, https://doi.org/10.1063/1.2889947.

[10] H. Kawarada, T. Yamada, D. Xu, H. Tsuboi, Y. Kitabayashi, D. Matsumura, M. Shibata, T. Kudo, M. Inaba, A. Hiraiwa, Durability-enhanced two-dimensional hole gas of C-H diamond surface for complementary power inverter applications, Sci. Rep. 7 (2017), 42368, https://doi.org/10.1038/srep42368.

[11] Electrical Properties of Semiconductor Surfaces. Daniel R. Frankl. Pergamon, New York, 1967, 310pp, n.d.

[12] Z. Chi, J.J. Asher, M.R. Jennings, E. Chikoidze, A. Pérez-Tomás, Ga2O3 and related ultra-wide bandgap power semiconductor oxides: new energy electronics solutions for CO_2 emission mitigation, Materials 15 (2022) 1164, https://doi.org/10.3390/ma15031164.

[13] E. Chikoidze, D.J. Rogers, F.H. Teherani, C. Rubio, G. Sauthier, H.J. Von Bardeleben, T. Tchelidze, C. Ton-That, A. Fellous, P. Bove, E.V. Sandana, Y. Dumont, A. Perez-Tomas, Puzzling robust 2D metallic conductivity in undoped β-Ga2O3 thin films, Mater. Today Phys. 8 (2019) 10–17, https://doi.org/10.1016/j.mtphys.2018.11.006.

[14] J. Lee, S. Ganguli, A.K. Roy, S.C. Badescu, Density functional tight binding study of **β** -Ga $_2$ O $_3$: Electronic structure, surface energy, and native point defects, J. Chem. Phys. 150 (2019), 174706, https://doi.org/10.1063/1.5088941.

[15] T.C. Lovejoy, E.N. Yitamben, N. Shamir, J. Morales, E.G. Villora, K. Shimamura, S. Zheng, F.S. Ohuchi, M.A. Olmstead, Surface morphology and electronic structure of bulk single crystal β-Ga2O3(100), Appl. Phys. Lett. 94 (2009), 081906, https://doi.org/10.1063/1.3086392.

[16] V.M. Bermudez, The structure of low-index surfaces of β-Ga2O3, Chem. Phys. 323 (2006) 193–203, https://doi.org/10.1016/j.chemphys.2005.08.051.

[17] R.M. Gazoni, L. Carroll, J.I. Scott, S. Astley, D.A. Evans, A.J. Downard, R.J. Reeves, M.W. Allen, Relationship between the hydroxyl termination and band bending at (2 ¯ 01) β − G a 2 O 3 surfaces, Phys. Rev. B. 102 (2020), 035304, https://doi.org/10.1103/PhysRevB.102.035304.

[18] J.E.N. Swallow, J.B. Varley, L.A.H. Jones, J.T. Gibbon, L.F.J. Piper, V.R. Dhanak, T. D. Veal, Transition from electron accumulation to depletion at β-Ga $_2$ O $_3$ surfaces: The role of hydrogen and the charge neutrality level, APL Mater. 7 (2019), 022528, https://doi.org/10.1063/1.5054091.

[19] Z. Yang, W. Chen, S. Kuang, Z. Sheng, J. Shi, D. Chen, M. Cui, H. Qi, K.H.L. Zhang, Crystal Phase, Electronic Structure, and Surface Band Bending of (In $_x$ Ga $_{1-x}$) $_2$ O $_3$ Alloy Wide-Band-Gap Semiconductors, Cryst. Growth Des. 22 (2022) 7325–7330, https://doi.org/10.1021/acs.cgd.2c00948.

[20] M. Razeghi, J. Lee, L. Gautam, J.-P. Leburton, F.H. Teherani, P.K. Amiri, V. P. Dravid, D. Pavlidis, Microstrip Array Ring FETs with 2D p-Ga2O3 Channels Grown by MOCVD, Photonics 8 (2021) 578, https://doi.org/10.3390/photonics8120578.

[21] S. Mu, M. Wang, H. Peelaers, C.G. Van de Walle, First-principles surface energies for monoclinic Ga $_2$ O $_3$ and Al $_2$ O $_3$ and consequences for cracking of (Al $_x$ Ga $_{1-x}$) $_2$ O $_3$, APL Mater. 8 (2020), 091105, https://doi.org/10.1063/5.0019915.

[22] A.M. Goodman, Semiconductors: *Electrical Properties of Semiconductor Surfaces*. Daniel R. Frankl. Pergamon, New York, 1967. xvi + 310 pp., illus. $13.50. International Series of Monographs on Semiconductors, vol. 7, Science 159 (1968), https://doi.org/10.1126/science.159.3818.970.b.

[23] J.H. Leach, K. Udwary, J. Rumsey, G. Dodson, H. Splawn, K.R. Evans, Halide vapor phase epitaxial growth of β-Ga $_2$ O $_3$ and α-Ga $_2$ O $_3$ films, APL Mater. 7 (2019), 022504, https://doi.org/10.1063/1.5055680.

[24] M. Yamaga, E.G. Víllora, K. Shimamura, N. Ichinose, M. Honda, Donor structure and electric transport mechanism in β − Ga 2 O 3, Phys. Rev. B. 68 (2003), 155207, https://doi.org/10.1103/PhysRevB.68.155207.

[25] N.T. Son, K. Goto, K. Nomura, Q.T. Thieu, R. Togashi, H. Murakami, Y. Kumagai, A. Kuramata, M. Higashiwaki, A. Koukitu, S. Yamakoshi, B. Monemar, E. Janzén, Electronic properties of the residual donor in unintentionally doped β-Ga2O3, J. Appl. Phys. 120 (2016), 235703, https://doi.org/10.1063/1.4972040.

[26] E. Chikoidze, H.J. von Bardeleben, K. Akaiwa, E. Shigematsu, K. Kaneko, S. Fujita, Y. Dumont, Electrical, optical, and magnetic properties of Sn doped α-Ga_2O_3 thin films, J. Appl. Phys. 120 (2016), 025109, https://doi.org/10.1063/1.4958860.

[27] H.J. von Bardeleben, J.L. Cantin, A. Parisini, A. Bosio, R. Fornari, Conduction mechanism and shallow donor properties in silicon-doped ε -G a 2 O 3 thin films: An electron paramagnetic resonance study, Phys. Rev. Mater. 3 (2019), 084601, https://doi.org/10.1103/PhysRevMaterials.3.084601.

[28] H.J. von Bardeleben, J.L. Cantin, Unusual conduction mechanism of n-type β-Ga $_2$ O $_3$: A shallow donor electron paramagnetic resonance analysis, J. Appl. Phys. 128 (2020), 125702, https://doi.org/10.1063/5.0023546.

[29] N.F. Mott, Conduction in non-crystalline systems: VIII. The highly correlated electron gas in doped semiconductors and in vanadium monoxide, Philos. Mag. 24 (1971) 935–958, https://doi.org/10.1080/14786437108217059.

[30] S. Luryi, B.I. Shklovskii, A.L. Efros, Electronic Properties of Doped Semiconductors, Springer Berlin Heidelberg, 2013. ⟨https://books.google.fr/books?id=OZXsCAAAQBAJ⟩.

[31] Low-Temperature Growth of Gallium Oxide Thin Films by Plasma-Enhanced Atomic Layer Deposition, J. Vac. Sci. Technol. a 38, 022404 (2020), (n.d.).

[32] R. Al-Gaashani, et al., Ceram. Int. 39 (2013) 2283–2292 (n.d.).

[33] C. Janowitz, V. Scherer, M. Mohamed, A. Krapf, H. Dwelk, R. Manzke, Z. Galazka, R. Uecker, K. Irmscher, R. Fornari, M. Michling, D. Schmeißer, J.R. Weber, J. B. Varley, C.G.V. de Walle, Experimental electronic structure of In $_2$ O $_3$ and Ga $_2$ O $_3$, N. J. Phys. 13 (2011), 085014, https://doi.org/10.1088/1367-2630/13/8/085014.

[34] M. Michling, D. Schmeißer, Resonant Photoemission at the O1s threshold to characterize β-Ga $_2$ O $_3$ single crystals, IOP Conf. Ser.: Mater. Sci. Eng. 34 (2012), 012002, https://doi.org/10.1088/1757-899X/34/1/012002.

[35] E. Chikoidze, A. Fellous, A. Perez-Tomas, G. Sauthier, T. Tchelidze, C. Ton-That, T. T. Huynh, M. Phillips, S. Russell, M. Jennings, B. Berini, F. Jomard, Y. Dumont, P-type β-gallium oxide: A new perspective for power and optoelectronic devices, Mater. Today Phys. 3 (2017) 118–126, https://doi.org/10.1016/j.mtphys.2017.10.002.

[36] P. Allongue, J.-N. Chazalviel, C. Henry de Villeneuve, F. Ozanam, Analysis of CapacitancePotential Measurements at the Silicon−Electrolyte Interface Revisited, J. Phys. Chem. C. 111 (2007) 5497–5499, https://doi.org/10.1021/jp068614z.

[37] R.G. Bates, J.B. MacAskill, "Standard potential of the silver-silver chloride electrode", Pure Appl. Chem. Vol. 50 (1978) 1701–1706 (n.d).

[38] C. Molto, A. Etcheberry, P.P. Grand, A.M. Goncalves, Study of photo-oxidized n-type textured silicon surface through electrochemical impedance spectroscopy, J. Electrochem. Soc. 167 (2020), 146505, https://doi.org/10.1149/1945-7111/abc0a6.

[39] Z. Zhang, J.T. Yates, Band Bending in Semiconductors: Chemical and Physical Consequences at Surfaces and Interfaces, Chem. Rev. 112 (2012) 5520–5551, https://doi.org/10.1021/cr3000626.

[40] Transport properties of topological insulators: Band bending, bulk metal-to-insulator transition, and weak anti-localization Matthew Brahlek a, Nikesh Koirala a, Namrata Bansal b, Seongshik Oh, Solid State Communications 215–216 (2015) 54–62., (n.d.).

[41] K. Barnham, D. Vvedensky. Low-Dimensional Semiconductor Structures: Fundamentals and Device Applications, 1st ed.,, Cambridge University Press,, 2001, https://doi.org/10.1017/CBO9780511624247.

[42] A. Mock, R. Korlacki, C. Briley, V. Darakchieva, B. Monemar, Y. Kumagai, K. Goto, M. Higashiwaki, M. Schubert, Band-to-band transitions, selection rules, effective mass, and excitonic contributions in monoclinic β − Ga 2 O 3, Phys. Rev. B. 96 (2017), 245205, https://doi.org/10.1103/PhysRevB.96.245205.

[43] A.K. Saikumar, S.D. Nehate, K.B. Sundaram, Review—RF Sputtered Films of Ga $_2$ O $_3$, ECS J. Solid State Sci. Technol. 8 (2019) Q3064–Q3078, https://doi.org/10.1149/2.0141907jss.

[44] R.E. Jones, K.M. Yu, S.X. Li, W. Walukiewicz, J.W. Ager, E.E. Haller, H. Lu, W. J. Schaff, Evidence for p -Type Doping of InN, Phys. Rev. Lett. 96 (2006), 125505, https://doi.org/10.1103/PhysRevLett.96.125505.

[45] P.D.C. King, T.D. Veal, P.H. Jefferson, C.F. McConville, H. Lu, W.J. Schaff, Variation of band bending at the surface of Mg-doped InGaN: Evidence of p -type conductivity across the composition range, Phys. Rev. B. 75 (2007), 115312, https://doi.org/10.1103/PhysRevB.75.115312.

[46] B.W. Licznerski, K. Nitsch, H. Teteryez, K. Wisniewski, The influence of Rh surface doping on anomalous properties of thick-film SnO2 gas sensors, Sens. Actuators B 79 (2001) 157 (n.d.).

[47] H. Teterycz, B.W. Licznerski, K. Nitsch, K. Wiśniewski, L.J. Golonka, Anomalous behaviour of new thick film gas sensitive composition, Sens. Actuators B 47 (1998) 153–157.

[48] M. Limpinsel, N. Farhi, N. Berry, J. Lindemuth, C.L. Perkins, Q. Lin, M. Law, An inversion layer at the surface of n-type iron pyrite, Energy Environ. Sci. 7 (2014) 1974, https://doi.org/10.1039/c3ee43169j.

[49] M. Krawczyk, R. Korbutowicz, R. Szukiewicz, P. Suchorska-Woźniak, M. Kuchowicz, H. Teterycz, P-type inversion at the surface of β-Ga2O3 epitaxial layer modified with Au nanoparticles, Sensors 22 (2022) 932, https://doi.org/10.3390/s22030932.

[50] J.J. Kolodziej, D. Wutke, J. Lis, N. Olszowska, Electronic structure of two-dimensional electron gases at differently prepared indium arsenide surfaces, Appl. Surf. Sci. 555 (2021), 149516, https://doi.org/10.1016/j.apsusc.2021.149516.

[51] S.M. Walker, F.Y. Bruno, Z. Wang, A. de la Torre, S. Riccó, A. Tamai, T.K. Kim, M. Hoesch, M. Shi, M.S. Bahramy, P.D.C. King, F. Baumberger, Carrier-Density

Control of the SrTiO $_3$ (001) Surface 2D Electron Gas studied by ARPES, Adv. Mater. 27 (2015) 3894–3899, https://doi.org/10.1002/adma.201501556.

[52] S. McKeown Walker, A. de la Torre, F.Y. Bruno, A. Tamai, T.K. Kim, M. Hoesch, M. Shi, M.S. Bahramy, P.D.C. King, F. Baumberger, Control of a Two-Dimensional Electron Gas on SrTiO 3 (111) by Atomic Oxygen, Phys. Rev. Lett. 113 (2014), 177601, https://doi.org/10.1103/PhysRevLett.113.177601.

[53] A.Y. Polyakov, V.I. Nikolaev, A.I. Pechnikov, E.B. Yakimov, S.Yu Karpov, S. I. Stepanov, I.V. Shchemerov, A.A. Vasilev, A.V. Chernykh, A. Kuznetsov, I.-H. Lee, S.J. Pearton, Two-dimensional hole gas formation at the κ-Ga2O3 /AlN heterojunction interface, J. Alloy. Compd. 936 (2023), 168315, https://doi.org/10.1016/j.jallcom.2022.168315.